Applied Catalysis B: Environmental 251 (2019) 17–24

Contents lists available at ScienceDirect

Applied Catalysis B: Environmental

journal homepage: www.elsevier.com/locate/apcatb

Selective oxidation of cyclohexane to cyclohexanol by BiOI under visible light: Role of the ratio (1 1 0)/(0 0 1) facet

David Contreras[a,b,c], Victoria Melin[a,c], Katherine Márquez[a], Gabriel Pérez-González[a,b], Héctor D. Mansilla[b], Gina Pecchi[b,c], Adolfo Henríquez[a,b,*]

[a] Renewable Resources Laboratory, Biotechnology Center, University of Concepción, University Campus, Concepción, Chile
[b] Faculty of Chemical Sciences, University of Concepción, University Campus, Concepción, Chile
[c] Millennium Nuclei on Catalytic Processes towards Sustainable Chemistry, Chile

ARTICLE INFO

Keywords:
Photocatalyst
BiOX
Bismuth oxyiodide
Oxofunctionalization
Facet
Cyclohexane

ABSTRACT

The development of semiconductors capable of photocatalytic activity under visible light is very important, because such materials are potentially useful for performing photocatalytic conversion under solar illumination. However, these processes are frequently unselective because they involve the production of free radicals. Reports suggest that the selectivity of the photocatalytic processes may be adjusted through modification of the structural parameters of the semiconductor photocatalysts by the preferential exposure of certain crystalline planes.

The present work focuses on the relationship between the preferential exposure of the (1 1 0) and (0 0 1) facets of bismuth oxyiodide and the cyclohexanol produced by the photocatalytic oxofunctionalization of cyclohexane. For this purpose, four bismuth oxyiodide photocatalysts (BiOI-4, BiOI-6, BiOI-10, and BiOI-12) were synthesized at different pH levels and characterized (via X-ray diffraction, diffuse reflectance spectroscopy, scanning electron microscopy, and the Brunauer–Emmett–Teller surface area). All BiOI photocatalysts showed higher selectivity for cyclohexanol. Additionally, a linear dependence between the cyclohexanol yield and peak intensity (1 1 0)/(0 0 1) ratio was established and related to the relative amount of hydroxyl radicals formed in the photocatalytic system.

1. Introduction

Selective activation of C(sp^3)—H bonds can be used to develop new strategies that are faster and easier than existing one for transforming relatively cheap raw materials into high-value organic molecules for use in the chemical, pharmaceutical and agricultural, industries. [1–3] Nevertheless, many of the current pathways for producing these products are environmentally harmful, offer low one-step conversion rates, and have a lower-than-desired selectivity with regard to their output [4].

The selective oxidation of cyclohexane to cyclohexanol and cyclohexanone is relatively important in the chemical industry. Annual cyclohexanol production is 10 thousand metric tons. These values do not include KA–oil (cyclohexanol/cyclohexanone) production for adipic acid synthesis. Worldwide annual cyclohexanone production is nearly 3.0 million metric tons, most of which is used for caprolactam production. [5] An ideal pathway for the oxidation of cyclohexane would yield only cyclohexanol and cyclohexanone with a conversion rate of 100%, using molecular oxygen as an oxidant reagent at room temperature and atmospheric pressure with a highly active catalyst.

Semiconductor photocatalysts have attracted increasing attention owing to their ability to destroy pollutants. When these materials are irradiated with photons with an energy equal to or higher than the bandgap, these photons are absorbed by the semiconductor and generate active photohole–photoelectron pairs. [6] Many semiconductor materials have been used as photocatalysts; among these, titanium dioxide is the most extensively used owing to its photoreactivity, biological and chemical stability, low cost, and non-toxicity [7,8]. Reports suggest that it is possible to produce cyclohexanol and cyclohexanone from cyclohexane in the liquid phase using titanium dioxide under mild conditions [9–12]. However, the bandgap of titanium dioxide (3.2 eV) implies the absorption of photons with wavelengths below 387 nm to promote photoelectrons from the valence band to the conduction band. As less than 5% of the solar flux at the surface of the Earth lies in the ultraviolet (UV) region, numerous efforts have focused on the development of new semiconductor materials for photocatalytic applications under visible light to enable more efficient use of the solar spectrum [13,14]. Recently, a strategy to extend the absorption spectra of TiO_2 to

* Corresponding author at: Renewable Resources Laboratory, Biotechnology Center, University of Concepción, University Campus, Concepción, Chile.
E-mail address: adohenriquez@udec.cl (A. Henríquez).

https://doi.org/10.1016/j.apcatb.2019.03.058
Received 30 September 2018; Received in revised form 19 March 2019; Accepted 20 March 2019
Available online 21 March 2019
0926-3373/

the visible light region and reduce recombination of photoelectrons and photoholes and promote dispersion of TiO_2 nanoparticles was developed by Zhao et al.; [15] this involved generating metal organic frameworks by coupling TiO_2 and organic linkers, such as NH_2MIL-125. However, the bandgap obtained for this photocatalyst was 2.70 eV, which meant wavelengths lower than 460 nm.

In the past decade, bismuth oxyhalides (BiOX, X = Cl, Br, I) have been extensively used because they show photocatalytic activity under visible light, in addition to having adequate chemical stability and desirable electrical and optical properties [16–19]. The band configuration, size, and morphology of these photocatalysts can be easily modified to obtain better photocatalytic performance by changing the conditions of synthesis, adding defects in their structure. Bismuth oxyhalides crystallize in tetragonal matlockite layered structures (space group P4/nmm), which consist of alternating $Bi_2O_2^{2+}$ sheets and double X^- slabs. [18,20,21] Among the bismuth oxyhalides, bismuth oxyiodide exhibits the narrowest bandgap (1.8–1.9 eV) and highest photocatalytic performance within the visible light region [22]. The narrow bandgap of bismuth iodide (BiOI) makes it an excellent material for solar applications [23]. Bismuth oxyiodide is of interest because of its low toxicity, stability in water, cheap and environmentally friendly synthesis, and notable photocatalytic activity. BiOI has been used in the photocatalytic process for the degradation of organic compounds including methyl orange [24], gallic acid [25], aniline [26], and phenol [27], and air pollutants such as nitric oxide [28].

Some authors have proposed a dependence between photocatalytic activity and the exposed facet of bismuth oxyiodide. He et al. [29] found that BiOI photocatalysts with hierarchical structures and an optimal ratio of (0 0 1) and (1 1 0) surfaces exhibited the best photocatalytic activity under visible light irradiation for phenol degradation. Pan et al. [30] found that bismuth oxyiodide with preferentially exposed (1 1 0) facets exhibited a higher photochemical performance than bismuth oxyiodide with dominant (0 0 1) facets in the degradation of bisphenol A. They attributed this observation to different radical formation mechanisms by the two bismuth oxyiodide photocatalysts. BiOI with preferentially exposed (1 1 0) facets could produce higher amounts of superoxide anion radicals, and it was only between these two photocatalysts that hydroxyl radicals could be directly produced. Additionally, Luo et al. [31] found that bismuth oxyiodide with exposed (1 1 0) facets exhibited higher visible light photocatalytic activity than irregular BiOI. Indeed, other authors have performed density functional theory calculations that suggest that the (0 0 1) facets of bismuth oxyhalide nanosheets possess the highest thermodynamic stability and photoactivity among the (0 0 1), (1 1 0), and (0 1 0) facets. Tuning the pH of the synthetic reaction of bismuth oxyhalides enables the facet-selective growth of the layered structure to achieve the desired facet exposure and thereby improve the photocatalytic performance of the material [32,33].

In previous work, we synthesized several photocatalysts to oxofunctionalize cyclohexane under visible light irradiation, and found that bismuth oxyiodide shows the greatest selectivity for cyclohexanol production. In the present work, we evaluate the effect of preferential exposition of the (1 1 0) and (0 0 1) facets on the performance of BiOI photocatalysts in the cyclohexane oxofunctionalization reaction under visible light irradiation. To this end, different samples of bismuth oxyiodide are synthesized by coprecipitation at different pH levels to obtain BiOI materials with different preferential facet orientations, in order to systematically study the relationship between the exposed facets and photocatalytic activity.

2. Experimental

2.1. Catalyst synthesis

Bismuth(III) nitrate pentahydrate, potassium iodide, cyclohexane, and cyclohexanol standards were purchased from Sigma–Aldrich and Merck. All reagents and solvents were used as received without further purification.

BiOI was prepared according to a modified synthetic procedure described by Wang et al. [15] $Bi(NO_3)_3$•$5H_2O$ (10 mmol) was dissolved in 100 mL of 1.57 mol L^{-1} acetic acid solution to obtain solution A. Solution B was prepared by dissolving 10 mmol potassium iodide in 100 mL of distilled water. Solution B was slowly added to solution A dropwise over 2 h to form a coloured precipitate. To direct facet formation in BiOI, the synthesis pH of the suspension was adjusted to 4, 6, 8, and 10 across different syntheses. The resulting solution was stirred for 1 h at room temperature. Then, the suspension was filtered, washed with distilled water, and fully dried at 70 °C. The samples were called BiOI-4, BiOI-6, BiOI-10, and BiOI-12, corresponding to synthesis pH of 4, 6, 10, and 12, respectively.

2.2. Catalyst characterization

X-ray diffraction (XRD) patterns of the samples were collected using a Bruker D4 ENDEAVOR X-ray diffractometer, using Cu K_α radiation as the source with a working voltage and current of 40 kV and 20 mA, respectively. The intensity of the diffraction peaks was recorded in the 5–80° (2θ) range in 0.02° increments with a counting time of 0.3 s per step.

The crystallite sizes of the semiconductor photocatalyst samples were estimated using the Debye–Scherrer formula (Eq. (1)), where D is the average crystallite size, K is a dimensionless shape factor (in this case, with a value of 0.94), λ is the X-ray radiation wavelength (Cu K_α = 0.154056 nm), β is the band broadening at half the maximum intensity, and θ is the diffraction angle.

$$D = \frac{K\lambda}{\beta\cos\theta} \quad (1)$$

UV–vis light (UV–vis) diffuse reflectance spectra of the bismuth oxyiodide samples were recorded with an Evolution 260 Bio UV–vis Spectrophotometer (Thermo Fisher Scientific Inc.) equipped with an integrating sphere in the range of 290–1100 nm, with a spectral resolution of 1 nm. The bandgap of the semiconductor photocatalyst was determined from a Tauc plot obtained from the UV–vis diffuse reflectance spectra. The relational expression proposed by Tauc, Davis, and Mott [34,35] (Eq. (2)) was used:

$$h\nu\alpha^{1/n} = A(h\nu - E_g) \quad (2)$$

where h is Planck's constant, ν is the vibration frequency, α is the absorption coefficient, E_g is the bandgap, and A is a proportional constant. The value of the exponent, n, denotes the nature of the simple transition. For an indirect allowed transition, n = 2. The α in the Tauc equation is substituted with the Kubelka–Munk function, $F(R_\infty)$. The morphology of the bismuth oxyiodide samples were obtained via scanning electron microscopy (SEM; JEOL model JSM-6380LV). Nitrogen adsorption isotherms at −196 °C were obtained using a TriStar II 3020 surface area and porosity analyser (Micromeritics Instrument Corporation).

2.3. Cyclohexane oxofunctionalization

The oxofunctionalization of cyclohexane was performed according the protocol used in previous work. [36] Briefly, 25 mL of cyclohexane was placed in a 50 mL two-necked round-bottomed flask fitted with a reflux condenser in the presence of 25 mg of catalyst (1 mg/mL) and 25 μL of nanopure water as source of generation of hydroxyl radicals.

For each reaction, the system was saturated with 1 atm of air for the duration of the reaction time (3 h). Photocatalytic oxidation reactions were carried out in a two-necked round-bottomed flask under external visible radiation generated by a 400 W metal halide lamp (Osram Powerstar HQI–E400 W/D Pro Daylight) [36]. The emission spectrum

of the lamp was recorded with a fluorescence spectrometer (LS–45, PerkinElmer) in luminescence mode. The radiant flux of the metal halide lamp was 2559 ± 44 μEinstein m^{-2} s^{-1}; this flux was recorded for 3 h using a QSPL-2100 radiometer (Biospherical Instruments Inc) with a quantum response from 400 to 700 nm. The temperatures inside the photocatalytic reactor reached 37 ± 2 °C.

2.4. Oxofunctionalized product quantification

To quantify the compounds obtained from the photocatalytic oxidation of cyclohexane, a 1.0 μL aliquot was removed from the reaction mixture and injected into a Series II gas chromatograph coupled to a flame ionization detector (Hewlett Packard Corporation, Palo Alto, California, USA). The analytes were separated in a crosslinked 5% diphenyl, 95% dimethylsiloxane column (Hewlett Packard Corporation, Palo Alto, California, USA). The temperature program was an isotherm set at 55 °C for 15 min. Nitrogen was used as the gas carrier at a constant flow of 1 mL/min. The temperature inlet was set to 250 °C, and the detector was set to 180 °C. The cyclohexanol concentrations of the reaction mixture aliquot were calculated by interpolating the area of the peaks of cyclohexanol in a standard curve. Carbon dioxide (CO_2) produced in the photocatalytic oxidation of cyclohexane catalysed by bismuth oxyiodide under visible light irradiation was determined by precipitation in $Ba(OH)_2$. For this determination, the reactor outlet was coupled to a CO_2 trapping system, where the gas produced in the reaction was bubbled into a test tube with $Ba(OH)_2$ 0.1 mol L^{-1} through a glass tube inlet. In order to avoid an increase in pressure inside of test tube, the rubber stopper was perforated with a hollow needle. In this system, all the CO_2 was precipitated as $BaCO_3$, [37,38] the amount of which was later quantified by turbidimetry [39] using a Hach turbidimeter (2100Q portable turbidimeter). The analytic method was validated by using a calibration curve with $BaCO_3$ (R^2 = 0.994). The CO_2 concentration was determined from this calibration curve.

2.5. In situ electron paramagnetic resonance experiments

To determine the role of the (1 0 1) facet of bismuth oxyiodide on the formation of hydroxyl radical during the oxidation of cyclohexane over the photoactivated surface of the photocatalysts, *in situ* electron paramagnetic resonance (EPR) measurements were performed with an EMX micro 6/1 Bruker ESR spectrometer working at the X-band, equipped with a Bruker Super High QE cavity resonator using *N*-tert-butyl-α-phenylnitrone (PBN) as a spin trap for this apolar system. A 1 mg quantity of each photocatalyst was dispersed in 1 mL of cyclohexane containing 10 mmol L^{-1} of PBN and 0.1% (v/v) nanopure water. The reaction was initiated by turning on the irradiation source. The reaction system was saturated with air during the reaction time. The reaction was carried out in an EPR sample tube (ER 221TUB/, 4 mm I.D.) inside the EPR cavity, irradiated with the 400 W metal halide lamp described above. The *in situ* measurement was performed at room temperature. Typical instrumental conditions were as follows: centre field, 3514 G; sweep width, 200 G; microwave power, 20 dB; modulation frequency, 100 kHz; time constant, 0.01 ms; sweep time, 30 s; modulation amplitude, 1.00 G; and receiver gain, 30 dB.

3. Results and discussion

3.1. Catalyst characterization

The structural and electronic properties of the synthesized photocatalysts are presented in Table 1, and the X-ray powder diffraction patterns are shown in Fig. 1. The XRD patterns of samples of bismuth oxyhalides synthesized at different pH levels were indexed to the tetragonal phase of BiOI (JCPDS Card No. 73–2062). All diffraction patterns of the BiOI samples exhibited intense signals at 29.7, 31.7, 45.4, and 55.2° (2θ), assigned to the (1 1 0), (1 0 2), (0 2 0), and (1 2 2) facets, respectively. The greatest variation in diffractograms was observed for the (0 0 1) facet (9.6°, 2θ). The predominance of the (0 0 1) facets decreased as the pH of the synthesis increased. This effect was also observed by Han et al., [40] who explained that under acidic conditions, the formation of (0 0 1) is predominant because the protons are absorbed more strongly on the O-terminated (0 0 1) facets than on the (1 1 0) surface, thus hindering the growth of the crystal in the (0 0 1) direction.

Table 1
Structural and electronic properties of the synthesized semiconductor photocatalysts.

Photocatalyst	Crystallite size[a] (nm)	BET surface area (m^2 g^{-1})	Pore size (nm)	Pore volume (cm^3 g^{-1})	Band gap[b] (eV)
BiOI-4	30.17	3.7	5.65	0.0052	1.85
BiOI-6	23.95	4.9	5.84	0.0071	1.90
BiOI-10	23.26	7.4	6.69	0.0123	1.91
BiOI-12	31.31	5.7	6.58	0.0093	1.90

BET, Brunauer–Emmett–Teller.
[a] Calculated from XRD measurements using the Scherrer equation.
[b] Calculated from the diffuse reflectance UV–vis spectra using the Kubelka–Munk function.

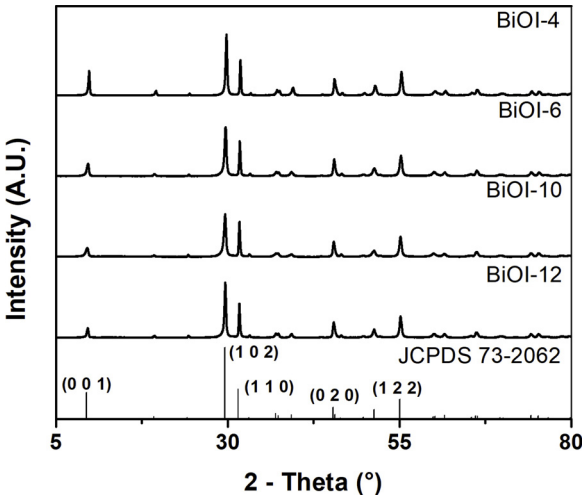

Fig. 1. XRD patterns of as-synthetized BiOI photocatalyst.

The performance of a semiconductor material as a photocatalyst is strongly influenced by its ability to absorb photons. This ability was evaluated by diffuse reflectance spectroscopy. The diffuse reflectance spectra of the BiOI samples are shown in Fig. 2. The bandgaps of the BiOI samples were determined by interpolation from the plot of the transformed Kubelka–Munk function versus the energy of the light absorbed by the BiOI photocatalysts (inset in Fig. 2). The calculated bandgaps for BiOI-4, BiOI-6, BiOI-10, and BiOI-12 were 1.85, 1.90, 1.91, and 1.90, respectively. Considering the closeness of the bandgap, this parameter could be constant across the synthesized BiOI photocatalysts. Hence, any differences between the reactivities of the BiOI samples must be attributed to other properties of the BiOI photocatalysts.

All samples of BiOI presented type II adsorption and desorption isotherms (Fig. 3), suggesting a non-porous presence or possibly macroporous materials. The specific areas were determined from the nitrogen adsorption–desorption isotherms. The specific surface areas (SSAs) of the BiOI samples were very small, ranging from 2.3 to 7.4 m^2 g^{-1}. These results were consistent with the fact that the BiOI samples corresponded to non-porous materials. Moreover, considering the instrumental error (± 5 m^2 g^{-1}), no significant differences in the SSAs between the BiOI samples were observed. Accordingly, any

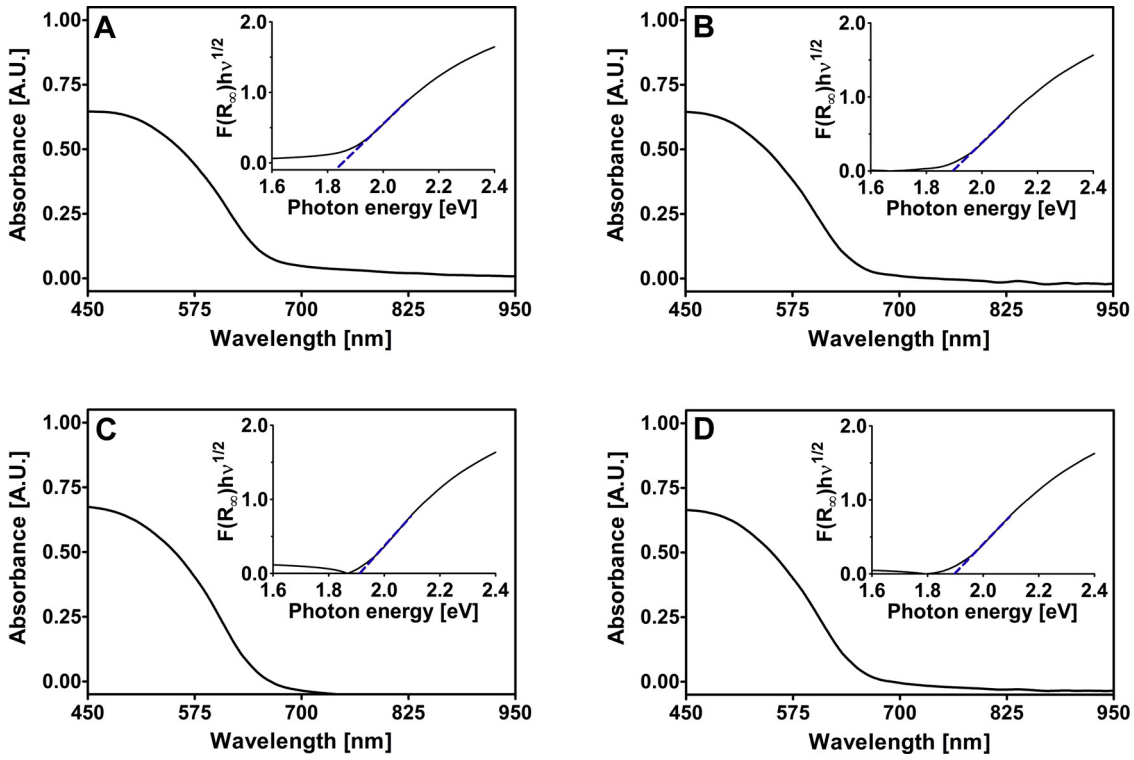

Fig. 2. UV–vis diffuse reflectance spectra of (A) BiOI–4, (B) BiOI–6, (C) BiOI–10 and (C) BiOI–12. Inset shows the Kubelka-Munk function vs photon energy curves.

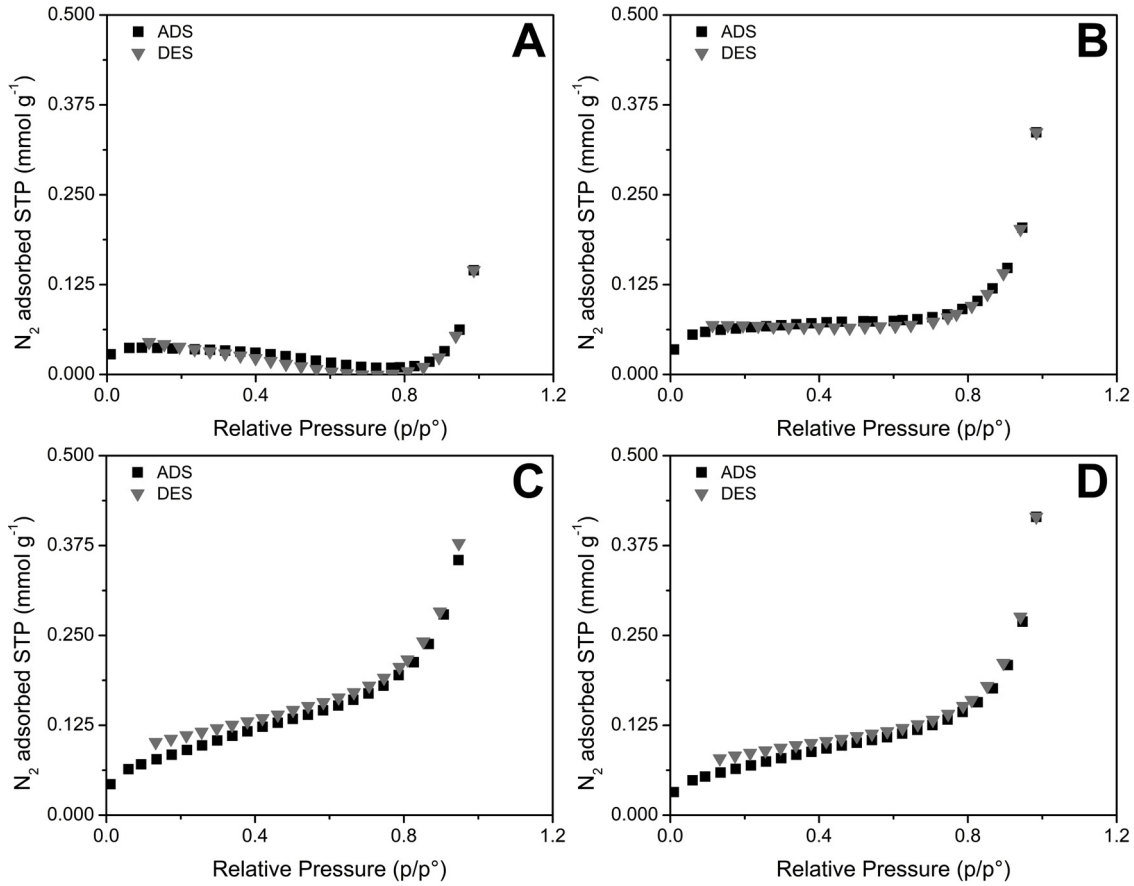

Fig. 3. Nitrogen adsorption and desorption isotherms for (A) BiOI-4, (B) BiOI-6, (C) BiOI-10, and (D) BiOI-12.

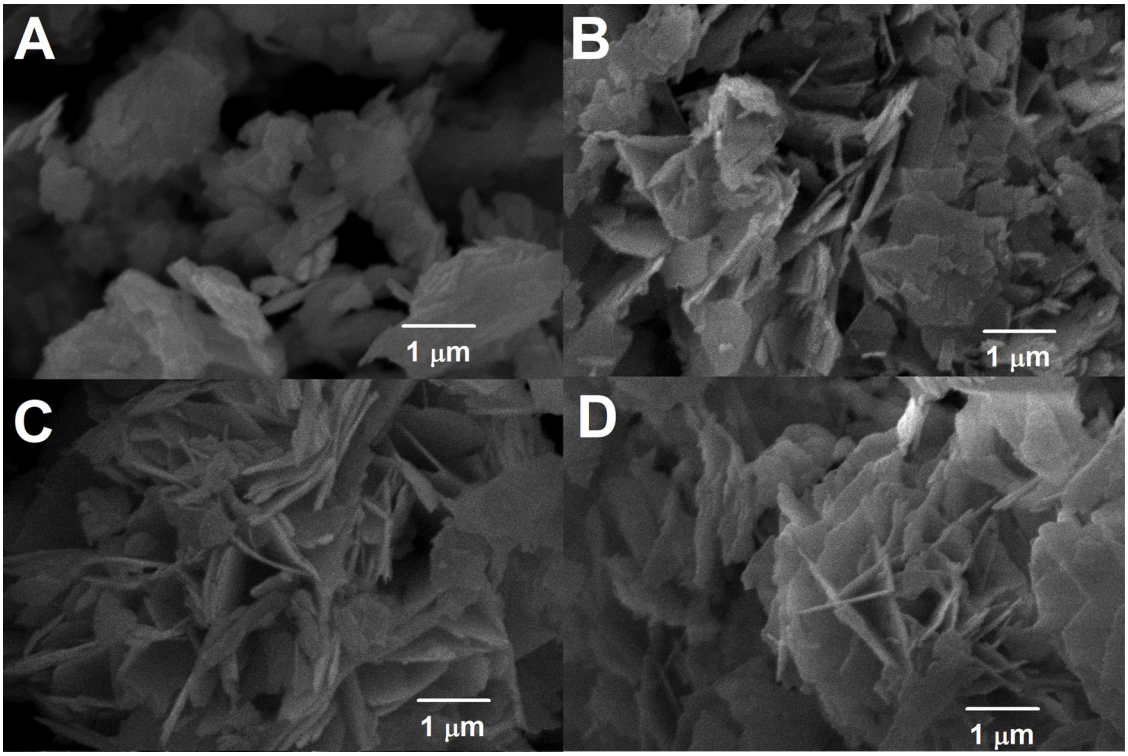

Fig. 4. SEM images of BiOI samples. (A) BiOI-4, (B) BiOI-6, (C) BiOI-10, and (D) BiOI-12.

differences in the reactivity of the synthesized BiOI photocatalysts were not due to this factor.

SEM images revealed that all the synthesized BiOI materials had a laminar structure (Fig. 4). The size of the nanosheets changed with the pH of the synthesis, but no trend was observed according to the conditions of synthesis (Table 1).

3.2. Cyclohexane oxofunctionalization

After 180 min of the photocatalytic oxofunctionalization reaction with all synthesized BiOI-based photocatalysts, only cyclohexanol, cyclohexanone, and CO_2 were detected as products. The cyclohexanol concentrations were quantified (Fig. 5). The minimum yield for cyclohexanol observed after 3 h of reaction was attained by BiOI-4 (0.85 ± 0.07 μmoles). The maximum yield for cyclohexanol was attained by BiOI-10 (2.10 ± 0.35 μmoles). The lowest yield of CO_2 was observed in the BiOI-10 system (0.22 ± 2.15) × 10^{-3} μmoles, while the highest was (6.07 ± 1.24) × 10^{-3} μmoles, produced by the BiOI-12 system.

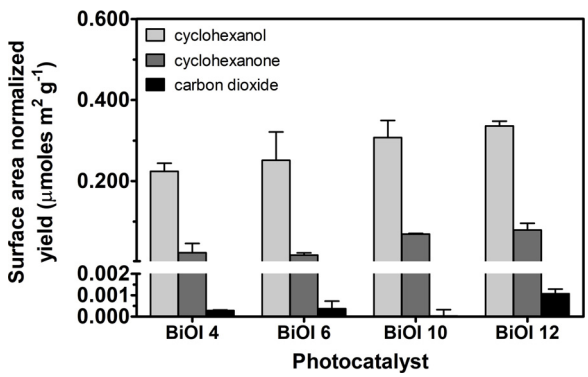

Fig. 5. Yield of cyclohexane oxofunctionalization catalysed by BiOI photocatalysts under visible light irradiation.

The effects of all the facets identified in the XRD patterns of the synthesized BiOI photocatalyst on cyclohexanol production were analysed. However, no correlation was found when the individual effects of these was considered. However, a linear dependence of the cyclohexanol yield with the peak intensity ratio of (1 1 0)/(0 0 1) was found (r = 0.87; Fig. 6). This result is in agreement with those reported by other researchers, [29] who indicated that the ratio of (1 1 0)/(0 0 1) facets was important to the photocatalytic activity of BiOI.

Table 2 shows a summary of studies on the selective photocatalytic oxidation of cyclohexane over different photocatalysts. In this work, the best conversion of cyclohexane to products was 0.0011%. To the best of our knowledge, the best conversion of cyclohexane under photocatalytic conditions was obtained by Zhao et al. with a conversion of 0.74% [15]. However, the photocatalyst prepared by Zhao et al. had an SSA of 571.2 $m^2 g^{-1}$, whereas the SSAs of the synthesized BiOI materials in this work were between 2.3 and 7.4 $m^2 g^{-1}$. Thus, the poor SSA of the BiOI photocatalyst may have been the cause of the low conversion of cyclohexane. Despite the low yields achieved by our photocatalyst, it should be noted that high selectivity, over 80% in each studied system, for the conversion of cyclohexane to cyclohexanol was observed.

3.3. Radical detection and its relationship with the reported mechanism

Given the relevance of •OH in the formation of cyclohexanol from cyclohexane oxofunctionalization, [36] the production of radical species formed during the photocatalytic oxofunctionalization of cyclohexane under visible light by BiOI photocatalysts were detected by spectroscopy, using PBN as a spin trap. The production of radicals was observed in the photoreactor though the typical triplet signal with hyperfine coupling constants of 8.1 G assigned to the PBNox (PhCON(O•)Bu^t, Fig. 7 A), which is usually believed to be formed by further oxidation of the PBN–OH spin adduct. Thereby, the formation of PBNox suggests the formation of •OH radical in the early stages of photocatalytic oxidation of cyclohexane over BiOI photocatalysts. The signal of PBNox increased with the pH of synthesis of BiOI. Moreover, the

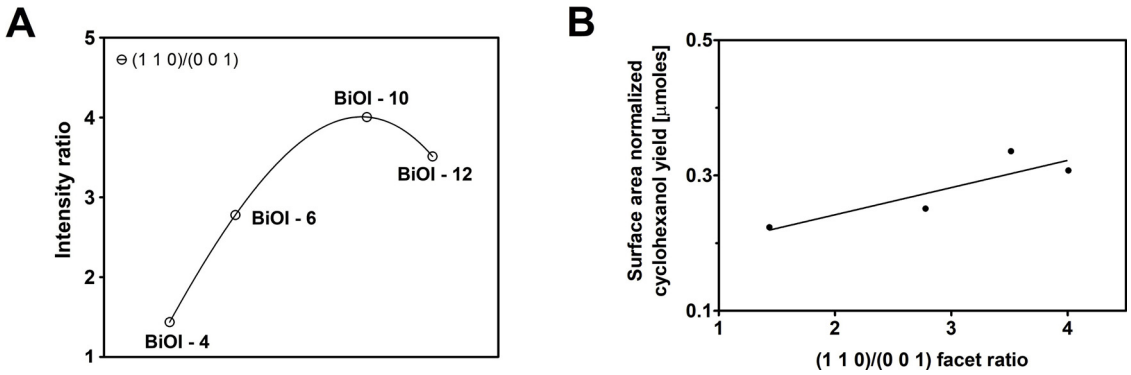

Fig. 6. (A) Peak intensity ratio (1 1 0)/(0 0 1) of BiOI facets. (B) Dependence of the cyclohexanol yield on the peak intensity ratio (1 1 0)/(0 0 1) for the BiOI photocatalysts.

Table 2
Selective photocatalytic oxidation of cyclohexane by BiOI synthetized as different pH levels and others reported photocatalysts.

Ref.	Catalyst	BET ($m^2 g^{-1}$)	Illumination source	Experimental conditions	Time (h)	Selectivity (%) [a]			CH conversion (%)[b]
						CHol	CHone	1/6 CO_2	
	BiOI-4 25 mg	2.3	400 W metal halides-lamp	24.975 mL C_6H_6 + 0.025 mL water	3	90.3	7.96	0.02	0.0004
	BiOI-6 25 mg	4.9	400 W metal halides-lamp	24.975 mL C_6H_6 + 0.025 mL water	3	93.5	6.19	0.03	0.0005
	BiOI-10 25 mg	7.4	400 W metal halides-lamp	24.975 mL C_6H_6 + 0.025 mL water	3	81.7	17.05	0.00	0.0011
	BiOI-12 25 mg	5.7	400 W metal halides-lamp	24.975 mL C_6H_6 + 0.025 mL water	3	80.7	18.06	0.04	0.0011
[10]	TiO_2 P25	50	125 W high pressure mercury-lamp (> 300 nm)	10 mL C_6H_6 with O_2 bubbling	3	5.00	83.00	12.00	0.3
[41]	Ultrafine TiO_2 30 mg	410	250 W high pressure mercury-lamp	10 mL C_6H_6 + 10 ml CH_3CN + HNO_3 1 mol	8	85.30	14.70	–	0.096
[42]	Nanosized TiO_2 30 mg	410	250 W high pressure mercury-lamp	10 mL C_6H_6 + 10 ml CH_3CN	3	84.50	14.90	0.60	0.097
[43]	TiO_2 P25 30 mg	–	solar simulator San-Ei Electric Co., Ltd. (1000 W m^{-2})	2 m L C_6H_6 + 18 mL O_2 saturated CH_3CN	6	5.20	55.50	39.30	0.33
[15]	NH_2-M125/P25-4 50 mg	571.2	300 W xenon-lamp (λ ≥ 420 nm)	10 mL C_6H_6 + 10 mL CH_3CN + 0.1 MPa O_2, 298 K	5	36.00	63.00	1.00	0.74

BET, Brunauer–Emmett–Teller.
[a] [(formed product) /([formed CHone) + (formed CHol + 1/6 (formed CO_2)] × 100%.
[b] [(formed CHone) + (formed CHol) + 1/6 (formed CO_2)]/(added CH) × 100%.

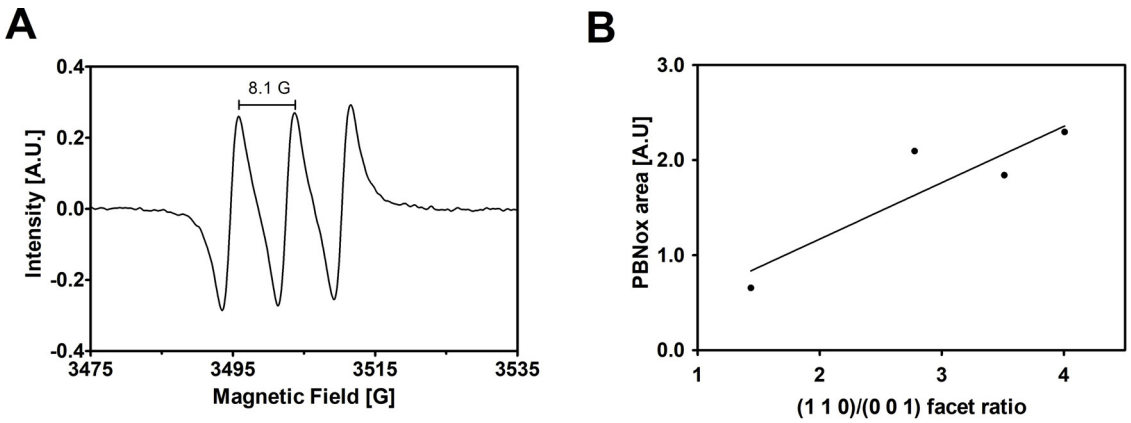

Fig. 7. (A) EPR signal observed for PBNox. (B) Dependence of the PBNox area and peak intensity ratio (1 1 0)/(0 0 1) for the BiOI photocatalysts.

amount of PBNox was linearly dependent on the (1 1 0)/(0 0 1) ratio (Fig. 7 B). These results are consistent with the observations of Pan et al. [30] that the (1 1 0) facet has the ability to generate hydroxyl radicals at difference of (0 0 1) facet of BiOI. On the other hand, we observed a linear dependence of cyclohexanol yield on the (1 1 0)/(0 0 1) facet ratio of BiOI materials.

Some authors refute the hypothesis of •OH formation in these photocatalytic systems due to redox incompatibility. The reported valence band maximum and conduction band minimum for bismuth oxyiodide are 0.60 and 2.39 eV, respectively. Consequently, the standard redox potential of the redox pair Bi^{V}/Bi^{III} is 1.83 V, and the standard redox potential of the •OH/ H_2O pair is 2.80 V. Therefore, the

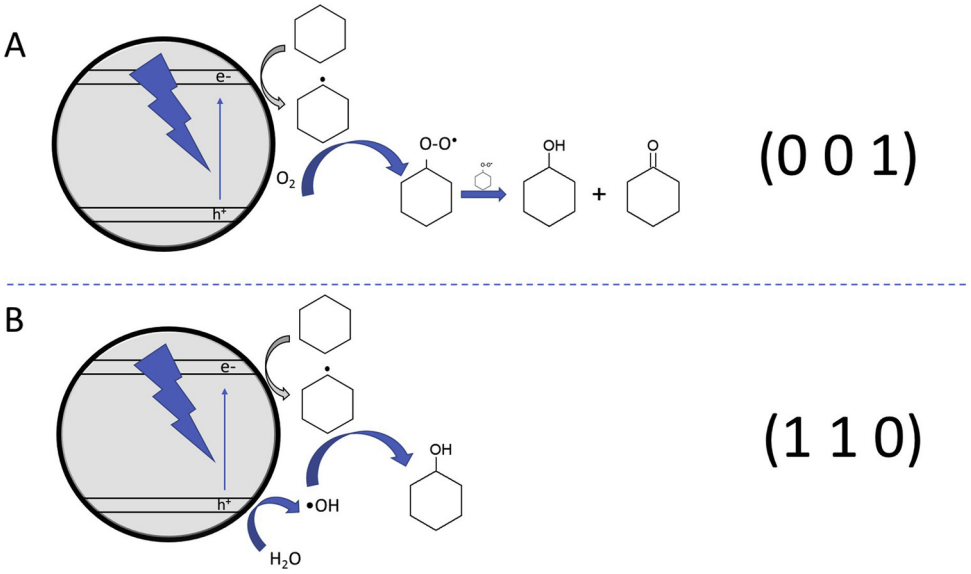

Fig. 8. Role of facet in the oxofunctionalization of cyclohexane (A) (0 0 1) facet and (B) (1 1 0) facet.

standard potential of the oxidation of H_2O to •OH by the Bi^{V}/Bi^{III} couple is −0.97 V which indicates a non-spontaneous reaction. Since the cyclohexane oxofunctionalization reactions were performed in inverse emulsions of water in cyclohexane, it is possible that photocatalytic reactions would occur in an aqueous medium,owing to the interfacial shear strength between water microdroplets and cyclohexane.

Based on the Nernst equation for equilibrium (E = 0), the dependence of log [•OH] on pH is shown in Eq. (3)

$$\log[\bullet OH] = pH - 16.4 \quad (3)$$

At equilibrium, the •OH concentration will be pH dependent. At pH 7.0, the maximum concentration of •OH will be 4×10^{-10} mol L^{-1}, reaching 4×10^{-3} mol L^{-1} at pH 14. Given that the local pH at the interface of the catalyst with water could be alkaline, it is reasonable to consider the possibility of the production of •OH. This analysis is in agreement with our previous report, [36] where empirical evidence of the production of •OH was obtained by EPR *in situ* in an experimental analysis of the oxofunctionalization of cyclohexane with BiOI photocatalysts.

To explain the high selectivity observed in the synthetized BiOI and its relationship with the (1 1 0)/(0 0 1) facet ratio, a proposed pathway for cyclohexane oxofunctionalization is detailed in Fig. 8 considering the reported properties of each facet and the mechanism of cyclohexane activation previously described in the literature. According to this pathway, the oxidation of cyclohexane in facet (0 0 1) is carried out by a mechanism of catalysis reported in the literature: the activation of a cyclohexane molecule over a semiconductor material with photocatalytic activity is caused by hydrogen abstraction by the photohole, yielding a cyclohexyl radical. The cyclohexanone is eventually formed by a disproportionate reaction of the cyclohexyl peroxyl radical formed in the reaction of cyclohexyl radical with the absorbed O_2 in the surface of the catalyst (Fig. 8A). The oxofunctionalization of cyclohexane in facet (1 1 0) is different since only the (1 1 0) facet is able to produce •OH [30]. Thus, in this facet, the •OH produced by photocatalytic oxidation of water inhibits the production of cyclohexanone, owing to this radical directly reacting with the cyclohexyl radical to form cyclohexanol (Fig. 8B) [36]. Higher selectivity towards cyclohexanol was observed in all the BiOI materials studied in this work, since all them had a portion of the (1 1 0) facet (Fig. 1). However, the photocatalyst with the highest ratio of (1 1 0)/(0 0 1) facets showed the best yield of cyclohexanol, which can be explained by greater inhibition of the disproportion reaction. Moreover, the difference in the proportion of oxygen atoms on the surface of the photocatalyst was facet dependent (1 1 0 = 1.94 O nm^{-2}; 0 0 1 = 6.27 O nm^{-2}) [40]. Thus, changes in the ratio of (1 1 0)/(0 0 1) facets in the BiOI photocatalyst produced a change in the charge of the surface, promoting the adsorption of cyclohexane in the surface of the photocatalyst with lower polarity, that is, with a higher ratio of (1 1 0)/(0 0 1) facets.

4. Conclusions

In this work a linear dependence was established between the intensity ratio (1 1 0)/(0 0 1) facets and cyclohexanol yield of photocatalytic oxofunctionalization yield under visible light. This dependence was directly related to the mechanisms that prevail in the oxidation process with this kind of semiconductor photocatalyst and the ability of the (1 1 0) planes to generate •OH. Otherwise, all BiOI photocatalysts showed higher selectivity for cyclohexanol than cyclohexanone.

Acknowledgements

This Special Issue is dedicated in honour of the retirement of Prof. César Pulgarin at the Swiss Federal Institute of Technology (EPFL, Switzerland), a key figure in the area of Catalytic Advanced Oxidation Processes. The author thanks the financial support given by CONICYT National Doctoral Fellowship21130450; FONDECYT1160100; Millennium Science Initiative of the Ministry of Economy, Development and Tourism, grant Nuclei on Catalytic Processes towards Sustainable Chemistry (CSC) and FONDAP Solar Energy Research Center, SERC–Chile15110019.

References

[1] M. Castellote, N. Bengtsson, Principles of TiO_2 photocatalysis, Appl. Titan. Dioxide Photocatal. to Constr. Mater., XII, State-of-the-Art Report of the RILEM Technical Committee 194-TDP, (2019), pp. 5–10 n.d.: pp..
[2] I. Prat, A. Company, V. Postils, X. Ribas, L. Que, J.M. Luis, M. Costas, The mechanism of stereospecific CH oxidation by Fe(Pytacn) complexes: bioinspired non-heme Iron catalysts containing cis-labile exchangeable sites, Chem. Eur. J. 19 (2013) 6724–6738, https://doi.org/10.1002/chem.201300110.
[3] C. Coperet, C.-H. Bond, Activation and organometallic intermediates on isolated metal centers on oxide surfaces, Chem. Rev. 110 (2010) 656–680, https://doi.org/10.1021/cr900122p.
[4] M.A. Gonzalez, S.G. Howell, S.K. Sikdar, Photocatalytic selective oxidation of hydrocarbons in the aqueous phase, J. Catal. 183 (1999) 159–162, https://doi.org/10.1006/jcat.1999.2395.
[5] W.B. Fisher, J.F. VanPeppen, Cyclohexanol-cyclohexanone, Van Nostrand's Encycl, John Wiley & Sons, Inc, Chem, 2005, https://doi.org/10.1002/0471740039.

vec0746.
[6] C. McCullagh, P.K.J. Robertson, M. Adams, P.M. Pollard, A. Mohammed, Development of a slurry continuous flow reactor for photocatalytic treatment of industrial waste water, J. Photochem. Photobiol. A Chem. 211 (2010) 42–46, https://doi.org/10.1016/j.jphotochem.2010.01.020.
[7] J.M.C. Robertson, P.K.J. Robertson, L.A. Lawton, A comparison of the effectiveness of TiO_2 photocatalysis and UVA photolysis for the destruction of three pathogenic micro-organisms, J. Photochem. Photobiol. A Chem. 175 (2005) 51–56, https://doi.org/10.1016/j.jphotochem.2005.04.033.
[8] A.J. Han, S.F. Chian, X.Y. Toy, J.L. Sun, S. Jaenicke, G.K. Chuah, Bismuth oxyiodide heterojunctions in photocatalytic degradation of phenolic molecules, Res. Chem. Intermed. 41 (2015) 9509–9520, https://doi.org/10.1007/s11164-015-1976-7.
[9] C.B. Almquist, P. Biswas, The photo-oxidation of cyclohexane on titanium dioxide: an investigation of competitive adsorption and its effects on product formation and selectivity, Appl. Catal. A Gen. 214 (2001) 259–271, https://doi.org/10.1016/S0926-860X(01)00495-1.
[10] W. Mu, J.M. Herrmann, P. Pichat, Room-Temperature Photocatalytic oxidation of liquid cyclohexane into cyclohexanone over neat and modified TiO_2, Catal. Lett. 3 (1989) 73–84, https://doi.org/10.1007/BF00765057.
[11] A. Sclafani, J.M. Herrmann, Comparison of the photoelectronic and photocatalytic activities of various anatase and rutile forms of titania in pure liquid organic phases and in aqueous solutions, J. Phys. Chem. 100 (1996) 13655–13661, https://doi.org/10.1021/jp9533584.
[12] P. Boarini, V. Carassiti, A. Maldotti, R. Amadelli, Photocatalytic oxygenation of cyclohexane on titanium dioxide suspensions: effect of the solvent and of oxygen, Langmuir 14 (1998) 2080–2085, https://doi.org/10.1021/la970384f.
[13] A. Martinez-de la Cruz, U.M. Garcia-Perez, S. Sepulveda-Guzman, Characterization of the visible-light-driven $BiVO_4$ photocatalyst synthesized via a polymer-assisted hydrothermal method, Res. Chem. Intermed. 39 (2013) 881–894, https://doi.org/10.1007/s11164-012-0602-1.
[14] Y.C. Lan, Y.L. Lu, Z.F. Ren, Mini review on photocatalysis of titanium dioxide nanoparticles and their solar applications, Nano Energy 2 (2013) 1031–1045, https://doi.org/10.1016/j.nanoen.2013.04.002.
[15] X. Zhao, Y. Zhang, P. Wen, G. Xu, D. Ma, P. Qiu, NH_2-MIL-125(Ti)/TiO_2 composites as superior visible-light photocatalysts for selective oxidation of cyclohexane, Mol. Catal. 452 (2018) 175–183, https://doi.org/10.1016/j.mcat.2018.04.004.
[16] S.L. Wang, L.L. Wang, W.H. Ma, D.M. Johnson, Y.F. Fang, M.K. Jia, Y.P. Huang, Moderate valence band of bismuth oxyhalides (BiOXs, X = Cl, Br, I) for the best photocatalytic degradation efficiency of MC-LR, Chem. Eng. J. 259 (2015) 410–416, https://doi.org/10.1016/j.cej.2014.07.103.
[17] W.D. Zhang, Q. Zhang, F. Dong, Visible-light photocatalytic removal of NO in air over BiOX (X = Cl, Br, I) single-crystal nanoplates prepared at room temperature, Ind. Eng. Chem. Res. 52 (2013) 6740–6746, https://doi.org/10.1021/ie400615f.
[18] X.Y. Qin, H.F. Cheng, W.J. Wang, B.B. Huang, X.Y. Zhang, Y. Dai, Three dimensional BiOX (X=Cl, Br and I) hierarchical architectures: facile ionic liquid-assisted solvothermal synthesis and photocatalysis towards organic dye degradation, Mater. Lett. 100 (2013) 285–288, https://doi.org/10.1016/j.matlet.2013.03.045.
[19] L. Zhao, Z.C. Liu, X.Q. Zhang, T. Cui, J.H. Han, K.Y. Guo, B. Wang, Y.J. Li, T.T. Hong, J.Q. Liu, Z.F. Liu, Three-dimensional flower-like hybrid BiOI-zeolite composites with highly efficient adsorption and visible light photocatalytic activity, RSC Adv. 4 (2014) 45540–45547, https://doi.org/10.1039/c4ra07049f.
[20] L. Ye, Y. Su, X. Jin, H. Xie, C. Zhang, Recent advances in BiOX (X = Cl, Br and I) photocatalysts: synthesis, modification, facet effects and mechanisms, Environ. Sci. Nano 1 (2014) 90, https://doi.org/10.1039/c3en00098b.
[21] X. Xiao, W.D. Zhang, Facile synthesis of nanostructured BiOI microspheres with high visible light-induced photocatalytic activity, J. Mater. Chem. 20 (2010) 5866–5870, https://doi.org/10.1039/c0jm00333f.
[22] S. Luo, C. Tang, Z. Huang, C. Liu, J. Chen, M. Fang, Effect of different Bi/Ti molar ratios on visible-light photocatalytic activity of BiOI/TiO_2 heterostructured nanofibers, Ceram. Int. 42 (2016) 15780–15786, https://doi.org/10.1016/j.ceramint.2016.07.043.
[23] N.T. Hahn, S. Hoang, J.L. Self, C.B. Mullins, Spray pyrolysis deposition and photoelectrochemical properties of n-Type BiOI nanoplatelet thin films, ACS Nano 6 (2012) 7712–7722, https://doi.org/10.1021/nn3031063.
[24] Q.S. Yan, Y.L. Zhao, M.M. Xu, Y.Y. Wang, Enhanced visible-light photocatalytic performance of various bismuth oxyiodide with 3D hierarchical microspheres architecture, J. Nanosci. Nanotechnol. 16 (2016) 7731–7737, https://doi.org/10.1166/jnn.2016.12585.
[25] A.C. Mera, C.A. Rodríguez, M.F. Meléndrez, H. Valdés, Synthesis and characterization of BiOI microspheres under standardized conditions, J. Mater. Sci. 52 (2017) 944–954, https://doi.org/10.1007/s10853-016-0390-x.
[26] M.M. Xu, Y.L. Zhao, Q.S. Yan, Degradation of aniline by bismuth oxyiodide (BiOI) under visible light irradiation, J. Environ. Sci. Manag. 20 (2017) 18–25.
[27] D.L. Qian, S.T. Zhong, S.Y. Wang, Y.R. Lai, N. Yang, W. Jiang, Promotion of phenol photodegradation based on novel self-assembled magnetic bismuth oxyiodide core-shell microspheres, RSC Adv. 7 (2017) 36653–36661, https://doi.org/10.1039/c7ra06116a.
[28] J.M. Montoya-Zamor, A. Martinez-de la Cruz, E.L. Cuellar, Enhanced photocatalytic activity of BiOI synthesized in presence of EDTA, J. Taiwan Inst. Chem. Eng. 75 (2017) 307–316, https://doi.org/10.1016/j.jtice.2017.03.031.
[29] R.A. He, J.F. Zhang, J.G. Yu, S.W. Cao, Room-temperature synthesis of BiOI with tailorable (001) facets and enhanced photocatalytic activity, J. Colloid Interface Sci. 478 (2016) 201–208, https://doi.org/10.1016/j.jcis.2016.06.012.
[30] M.L. Pan, H.J. Zhang, G.D. Gao, L. Liu, W. Chen, Facet-dependent catalytic activity of nanosheet-assembled bismuth oxyiodide microspheres in degradation of bisphenol a, Environ. Sci. Technol. 49 (2015) 6240–6248, https://doi.org/10.1021/acs.est.5b00626.
[31] S.Q. Luo, J.W. Chen, Z.H. Huang, C. Liu, M.H. Fang, Controllable synthesis of titania-supported bismuth oxyiodide heterostructured nanofibers with highly exposed (110) bismuth oxyiodide facets for enhanced photocatalytic activity, ChemCatChem 8 (2016) 3780–3789, https://doi.org/10.1002/cctc.201601047.
[32] S. Bai, L.L. Wang, Z.Q. Li, Y.J. Xiong, Facet-engineered surface and interface design of photocatalytic materials, Adv. Sci. 4 (2017), https://doi.org/10.1002/advs.201600216.
[33] J. Li, Y. Yu, L.Z. Zhang, Bismuth oxyhalide nanomaterials: layered structures meet photocatalysis, Nanoscale 6 (2014) 8473–8488, https://doi.org/10.1039/c4nr02553a.
[34] J. Tauc, R. Grigorovici, A. Vancu, Optical properties and electronic structure of amorphous germanium, Phys. Status Solidi 15 (1966) 627–637, https://doi.org/10.1002/pssb.19660150224/abstract.
[35] E.A. Davis, N.F. Mott, Conduction in non-crystalline systems V. Conductivity, optical absorption and photoconductivity in amorphous semiconductors, Philos. Mag. 22 (1970) 903–922, https://doi.org/10.1080/14786437008221061.
[36] A. Henriquez, H.D. Mansilla, A.M. Martinez-de la Cruz, J. Freer, D. Contreras, Selective oxofunctionalization of cyclohexane over titanium dioxide-based and bismuth oxyhalide (BiOX, X=Cl-, Br-, I-) photocatalysts by visible light irradiation, Appl. Catal. B Environ. 206 (2017) 252–262, https://doi.org/10.1016/j.apcatb.2017.01.022.
[37] D.D. Van Slyke, The determination of carbon dioxide in carbonates, J. Biol. Chem. 36 (1918) 351–354 http://www.jbc.org/content/36/2/351.short.
[38] A.G. Malygin, V.D. Ponomareva, Simple chemical method for the determination of carbon dioxide in air, J. Anal. Chem. 62 (2007) 16–23, https://doi.org/10.1134/S1061934807010054.
[39] J. Akhoundzadeh, M. Costas, I. Lavilla, M. Chamsaz, C. Bendicho, Miniaturized and green method for determination of chemical oxygen demand using UV-induced oxidation with hydrogen peroxide and single drop microextraction, Microchim. Acta 180 (2013) 1029–1036, https://doi.org/10.1007/s00604-013-1024-5.
[40] A.J. Han, J.L. Sun, X.H. Lin, C.H. Yuan, G.K. Chuah, S. Jaenicke, Influence of facets and heterojunctions in photoactive bismuth oxyiodide, RSC Adv. 5 (2015) 88298–88305, https://doi.org/10.1039/c5ra18236k.
[41] B. Su, Y. He, X. Li, E. Lin, Q. Li, Photocatalytic oxidation of cyclohexane on ultrafine TiO_2 particles, Indian J. Chem. Sect. A Inorg. Phys. Theor. Anal. Chem. 36 (1997) 785–788.
[42] X. Li, X. Quan, C. Kutal, Synthesis and photocatalytic properties of quantum confined titanium dioxide nanoparticle, Scr. Mater. 50 (2004) 499–505, https://doi.org/10.1016/j.scriptamat.2003.10.031.
[43] H. Hattori, Y. Ide, S. Ogo, K. Inumaru, M. Sadakane, T. Sano, Efficient and Selective Photocatalytic Cyclohexane Oxidation on a Layered Titanate Modified with Iron Oxide under Sunlight and CO2 Atmosphere, ACS Catal. 2 (2012) 1910–1915, https://doi.org/10.1021/cs300339f.